Confinement properties of 2D porous molecular networks on metal surfaces

Müller, Kathrin; Enache, Mihaela; Stöhr, Meike

Published in:
Journal of Physics: Condensed Matter

DOI:
10.1088/0953-8984/28/15/153003

Publication date:
2016

Confinement properties of 2D porous molecular networks on metal surfaces

2016 J. Phys.: Condens. Matter 28 153003

(http://iopscience.iop.org/0953-8984/28/15/153003)

IOP Publishing Journal of Physics: Condensed Matter
J. Phys.: Condens. Matter **28** (2016) 153003 (16pp) doi:10.1088/0953-8984/28/15/153003

Topical Review

Confinement properties of 2D porous molecular networks on metal surfaces

Kathrin Müller[1,2], **Mihaela Enache**[1] and **Meike Stöhr**[1]

[1] Zernike Institute for Advanced Materials, University of Groningen, Nijenborgh 4, 9747AG Groningen, The Netherlands
[2] Max Planck Institute for Solid State Research, Heisenbergstr. 1, 70569 Stuttgart, Germany

E-mail: k.mueller@fkf.mpg.de and m.a.stohr@rug.nl

Received 6 November 2015, revised 8 February 2016
Accepted for publication 22 February 2016
Published 16 March 2016

Abstract

Quantum effects that arise from confinement of electronic states have been extensively studied for the surface states of noble metals. Utilizing small artificial structures for confinement allows tailoring of the surface properties and offers unique opportunities for applications. So far, examples of surface state confinement include thin films, artificial nanoscale structures, vacancy and adatom islands, self-assembled 1D chains, vicinal surfaces, quantum dots and quantum corrals. In this review we summarize recent achievements in changing the electronic structure of surfaces by adsorption of nanoporous networks whose design principles are based on the concepts of supramolecular chemistry. Already in 1993, it was shown that quantum corrals made from Fe atoms on a Cu(1 1 1) surface using single atom manipulation with a scanning tunnelling microscope confine the Shockley surface state. However, since the atom manipulation technique for the construction of corral structures is a relatively time consuming process, the fabrication of periodic two-dimensional (2D) corral structures is practically impossible. On the other side, by using molecular self-assembly extended 2D porous structures can be achieved in a parallel process, i.e. all pores are formed at the same time. The molecular building blocks are usually held together by non-covalent interactions like hydrogen bonding, metal coordination or dipolar coupling. Due to the reversibility of the bond formation defect-free and long-range ordered networks can be achieved. However, recently also examples of porous networks formed by covalent coupling on the surface have been reported. By the choice of the molecular building blocks, the dimensions of the network (pore size and pore to pore distance) can be controlled. In this way, the confinement properties of the individual pores can be tuned. In addition, the effect of the confined state on the hosting properties of the pores will be discussed in this review article.

Keywords: porous networks, electron confinement, scanning tunnelling microscopy, scanning tunnelling spectroscopy, molecular self-assembly

(Some figures may appear in colour only in the online journal)

1. Introduction

Surfaces and interfaces play an important role in many technological processes and applications like catalysis, corrosion protection, tribology, sensors, electronic devices, computer industry and many more. Often the chemical and electronic properties of surfaces and interfaces deviate significantly from the bulk properties of the materials due to the missing bonding partners at the surfaces. Recent examples are topological insulators [1] and nanoparticles [2, 3], besides the well-known

surface states of transition metal surfaces, which will be the focus of this review. Generally, the creation of a surface from a 3D crystalline material often leads to a change of its electronic and/or structural properties. At the surface, so-called surface states can exist, which appear due to the broken symmetry perpendicular to the surface and which decay exponentially both into vacuum and into the bulk, i.e. they are not degenerate with a bulk state. On the other hand, surface resonances are obtained when a surface state and a bulk state are degenerate. Their amplitude is enhanced at the surface while they behave like Bloch states in the bulk. Generally, one distinguishes between Shockley [4] and Tamm [5] surface states while it is only the mathematical approach that differs (nearly free electron approximation for Shockley states and tight binding approach for Tamm states) and not a physical distinction. Especially the Shockley surface states of gold, silver and copper, which are located in the band gaps of the projected bulk band structure (the surface Brillouin zone) and exhibit a free-electron-like parabolic band dispersion, have received much attention from the scientific community. These Shockley surface states react very sensitive to surface perturbations like adsorption of atoms or molecules, disorder or external electric fields [6]. With angle-resolved photoelectron spectroscopy (ARPES) and inverse photoemission spectroscopy (IPES) it is possible to map the occupied and the unoccupied band structure parallel to the surface, respectively [6–14]. Besides the mapping of surface states in reciprocal space by ARPES and IPES, real space investigations of surface states can be done by scanning tunnelling microscopy (STM). Here the fact that surface state electrons are scattered at defects like step edges, adatoms or vacancies leading to an interference of the incoming and outgoing electron waves is used to visualize the surface states, i.e. use is made of the so-called Friedel oscillations [15–17]. Due to its high spatial resolution and the possibility to map occupied and unoccupied electronic states in real space, STM is one of the most versatile tools to investigate electronic surface properties. With the STM it is not only possible to map the energy minimum of the surface states via scanning tunnelling spectroscopy (STS) but by 2D Fourier transformation of STM images taken at energies close to the Fermi level also the Fermi surface contour can be mapped [18]. Furthermore, it is possible to derive the parabolic dispersion of the surface state in reciprocal space by taking differential conductance (dI/dV) maps at different voltages. In this way, the wavelength of the Friedel oscillations (λ_F) can be directly measured and this is used to calculate the Fermi wave vector $k_F = \frac{2\pi}{\lambda_F}$ [15, 19–21]. However, it has to be noted that adequate care has to be taken when interpreting dI/dV maps taken under constant-current conditions. The reason is that the tunnelling matrix elements depend exponentially on the tip-sample distance and thus, dI/dV maps of surfaces with a strong surface and/or work function corrugation might be perturbed [21–25].

This review paper is organized as follows: First a brief overview on the interaction between surface states and adsorbates will be given, followed by a short description of molecular self-assembly with a special focus on porous networks. Additionally, theoretical methods to calculate the confinement of surface state electrons will be described. Afterwards, several examples of the surface state confinement with supramolecular porous networks built by metal coordination, hydrogen bonding and covalent bonding will be presented. That is followed by three examples of the influence of the confined states onto the adsorbates trapped in the pores of the honeycomb networks. Finally a brief outlook will be given.

2. Interaction of surface states with adsorbates

It is well-known that adsorbates can strongly interact with the surface states, which can either lead to a shift of the surface state due to specific adsorbate-substrate interactions [6, 26–29] or to a complete quenching of the surface state [6, 30, 31]. On the other hand the surface states can also strongly modify the adsorbate behaviour [32, 33]. For transition metal (1 1 1) surfaces it was shown that the distance between adatoms like Cu/Cu(1 1 1), Co/Cu(1 1 1), Co/Ag(1 1 1), Ce/Ag(1 1 1) and impurities on Cu(1 1 1) exhibits an oscillatory behaviour with a periodicity of $\lambda_F/2$ and with a decay of $1/r^2$, where r is the distance between neighbouring adatoms [33–38]. Monte-Carlo simulations and *ab initio* density functional theory (DFT) calculations confirmed that the scattering of the surface state electrons by the adsorbates leads to an oscillation in the long-range interaction potential parallel to the surface, which mediates the observed long-range ordering of adsorbates [34, 39–42]. A comparable finding was reported for the spacing between bromine adatom islands, which form a $(\sqrt{3} \times \sqrt{3})$ R30° superlattice on Cu(1 1 1) after annealing to 600 K and which exhibit an average distance between the islands that equals half the Fermi wavelength of the surface state oscillations [43].

A similar behaviour was found for molecular adsorbates. For example, CO was found to preferentially adsorb close to the minima of the standing wave pattern on Ag(1 1 1) [44]. For STM measurements for CS_2 on Au(1 1 1) it was observed that due to tip molecule interactions at low positive tip biases, which are comparable to the molecule-substrate interaction strength, the residence time of the molecules can be enhanced at the areas with the highest density of states of the standing wave patterns [45]. The stronger interaction with areas of high density of states was explained by the electrophilic nature of the CS_2 molecules. Even for large organic molecules, surface state effects were found to be responsible for the structure formation of the molecular overlayer. For cobalt-phthalocyanines adsorbed on Cu(1 1 1), the self-assembled coverage dependent patterns are strongly influenced by the quantum interference of the Cu(1 1 1) surface state electrons leading to arrays of disordered molecules with an average distance of 2.1 nm for 0.5 monolayers (ML), 1D chains separated by 2.1 nm for 0.7 ML and a complex Kagomé lattice for 0.8 ML exhibiting again intermolecular distances of 2.1 nm [46]. However, for molecules exhibiting a strong dipole like tris-(2-phenylpyridine)iridium(III) the repulsive intermolecular interactions were found to dominate over the surface state mediated attractive interactions and thus, the intermolecular distances cannot

be related to the wavelength of the Friedel oscillations of the Cu(1 1 1) Shockley surface state [47].

Besides the influence of the surface state on the adsorption behaviour and arrangement of adsorbates on surfaces, there are also many examples how the surface state is influenced and even can be manipulated by adsorbates. One of the most prominent examples is the arrangement of 48 iron atoms into a circular corral on Cu(1 1 1), as demonstrated by Crommie *et al* [48, 49], which led to a lateral confinement of the Cu(1 1 1) surface state. STS within this corral revealed several discrete resonances which agree very well with the eigenstates of the electrons calculated for a round 2D particle in a box system. Since confinement is not restricted to circular corrals this phenomenon has been also studied for triangular, square, rectangular and oval corrals prepared by atom-by-atom manipulation with a STM [49–51]. The manipulation of the electronic states inside the corral can be done by positioning metal adatoms at particular places. The placement of a Mn adatom in the centre of a quantum corral consisting of Mn atoms strongly influences the electronic structure in the centre showing nodes where have been maxima in the empty corral and vice versa. This was explained by the strong hybridization between the Mn atom and the surface electronic states and could be also modelled by a simple scattering model [50, 52, 53]. Manoharan *et al* showed that placing a Co atom at one of the focal points of an elliptical quantum corral leads to Kondo resonances not only at the atom but also at the empty focal point resulting in a so-called quantum mirage [51]. This was also confirmed theoretically by Stepanyuk *et al* [54, 55]. Moreover, confinement effects due to artificially created 1D resonators were investigated. By the creation of a 1D resonator consisting of two parallel Cu chains on Cu(1 1 1), the surface state can be confined leading to 1D standing wave patterns. The diffusion of individual Cu atoms within this resonator is strongly anisotropic with higher diffusion parallel to the 1D grating [56]. Furthermore, it was also shown that artificially constructed 1D chains from Au, Ag or Pd atoms develop a 1D band structure, which depends on the length and the composition of the chains [57–60].

Besides the confinement of surface state electrons in artificial 1D or 2D structures made from adatoms, it was reported that electrons can be confined in 2D structures like vacancy or adatom islands. For example for hexagonal vacancy islands on Cu(1 1 1), it was shown experimentally as well as theoretically that the local density of states (LDOS) of the islands depends on their size. The results can be reproduced by assuming scattering at the inner sides of a Cu corral structure to model scattering at the monolayer high edge of the vacancy island [61]. On the other hand, Crampin *et al* [52] as well as Kröger *et al* [62] reported that the line width of confined electronic states of vacancy islands on Ag(1 1 1) is only weakly affected by the geometry of the vacancies and that the life time is determined by lossy boundary scattering. A similar confinement was reported for Ag adatom islands on Ag(1 1 1). By comparing theoretical and experimental data it could be shown that the effective boundary of the confining Ag islands lies a constant distance beyond the position of the outermost Ag atoms in the Ag islands; this distance is independent of the island size [20, 63]. Another approach to create vacancy islands of different sizes in a controlled manner is to make artificial holes in a 2D self-assembled molecular island by STM manipulation of single molecules. This was done for tetraphenylporphyrins on Ag(1 1 1) [64]. With increasing size of the vacancy the minimum of the confined electronic state was observed to shift towards higher binding energy. In addition, by creating 1D structures of neighbouring vacancies the influence of created quantum well states on each other can be studied resulting in the formation of a 1D band.

Instead of using atom-by-atom manipulation with the STM for the preparation of low dimensional quantum structures, it is also possible to create artificial quantum well structures by molecular self-assembly. For example the self-assembly of methionine molecules on a Ag(1 1 1) surface leads to regular 1D gratings, which confine the surface state electrons in-between the molecular rows [65, 66]. Deposition of Fe atoms on the free metal area between the molecular rows changed the electronic structure to a 0D confinement. Furthermore, the self-alignment of Co and Fe adatoms, respectively, in the molecular gratings results in their regular distribution with an average separation of about 2.5 nm. This observed long-range interaction is due to the electronic structure of the Ag surface [65].

3. Molecular self-assembly and porous networks

Molecular self-assembly is one of the most versatile tools to build highly ordered organic layers in a bottom-up manner. It employs the concepts from supramolecular chemistry [67], where organic building blocks are held together by non-covalent interactions like hydrogen bonding [68–71], dipolar coupling [72–74], metal-coordination [75–77], or π–π stacking [78]. Due to the often relatively weak forces between the molecular building blocks, bond breaking and reformation are possible until the equilibrium structure is formed. Therefore, those structures are generally highly defect-free and sometimes even self-healing, which makes them ideal candidates for possible applications in electronic devices.

By using the chemistry 'tool box', organic molecules with specific ligands at predefined positions can be synthesized, which can be used to form 0D clusters [79, 80], 1D wires [81, 82], or 2D extended (porous) networks on surfaces [83, 84]. For a number of different reasons, porous networks are especially interesting as they can be used to host guest molecules, to study their dynamics, and to manipulate guest molecules with the STM. Furthermore, they are expected to show specific catalytic properties, i.e. to function as 'nanoreactors' [85–87]. The prototypical porous network held together by triple hydrogen bonding between 3,4,9,10-perylenetetracarboxylic diimide (PTCDI) and 1,3,5-triazine-2,4,6-triamine (melamine) was first reported on a silver terminated Si surface [69]. Similar PTCDI/melamine networks have been subsequently prepared on Au/mica [88], epitaxial graphene [89], highly-oriented pyrolytic graphite (HOPG), hexagonal boron nitride and molybdenum disulphide by deposition of the molecular building blocks from solution [90]. Besides the use of two molecules having complementary recognition sites, also molecules exhibiting self-complementary groups like carboxylic

groups are of great interest. For example the porous network formed by trimesic acid (TMA) and its larger 'relative' 1,3,5-benzene-tribenzoic acid (BTB) have been studied extensively on various surfaces like HOPG [91] and Au(1 1 1) [92, 93].

Recently, porous networks stabilized by metal-coordination gained increasing attention because the bonding—and thus, the mechanical stability—is generally stronger compared to hydrogen bonded networks [94]. Frequently, transition metal atoms like Co [95, 96], Fe [97–99], Cu [100], Ni [101] or rare earth metal atoms like Ce [102] are deposited onto the molecule-covered surfaces where they act as coordinating metal centres for the formation of the metal organic frameworks. Besides, native metal atoms from the substrate, onto which the molecules are deposited, can be used as the metal-coordination centres. This has been reported for example for Cu [79, 103] or Au [104–106] substrates. By the choice of the coordination metal atom, two-fold (Cu, Fe) [79], three-fold (Co) [95, 96] four-fold (Fe) [107] and five-fold (Ce) [102] coordination networks can be created, while by the choice of the molecular building blocks the sizes of the coordination networks are determined.

4. Theoretical considerations

In their pioneering work on the confinement of the Cu surface state electrons by a circular corral made from Fe atoms [48], Crommie *et al* also provided a qualitative description of the standing wave patterns observed inside the corral. By solving the Schrödinger equation for a particle in a hard wall box, the eigenstates and thus, the eigenenergies were determined. It should be noted that in order to describe the changes in the standing wave pattern upon scattering at the Fe adatoms as accurately as possible, a phase shift of the scattered wave has to be taken into account. The eigenstates inside a round 2D box having radius r are $\psi_{n,l}(\rho,\ \phi) \propto J_l(k_{n,\,l}\rho)\mathrm{e}^{\mathrm{i}l\phi}$ with n, l as main and angular momentum quantum number of an electron in a box, wavenumber $k_{n,l} = z_{n,l}/r$ and energy $E_{n,l} = \hbar^2 k^2_{n,l}/(2m^*)$. Here m^* is the effective mass of a surface state electron, J_1 is the lth order Bessel function and $z_{n,l}$ is the nth zero crossing of $J_l(z)$. Comparing experiment and simulation revealed that the eigenergies are reasonably well described (for the higher states deviations are present) while the model cannot account for the finite line width of the measured peaks. As possible reasons for the energy discrepancies as well as the broadening mechanism, transmission through the Fe adatoms (along the surface), scattering into the bulk (perpendicular to the surface) and inelastic scattering are given.

Soon after the first experimental realisation of the quantum corrals, Heller *et al* [108, 109] and Fiete *et al* [110] provided a theoretical description of them. To describe the LDOS inside the quantum corral which is obtained when taking dI/dV maps with the STM, multiple scattering theory was applied. The underlying physical principle can be envisioned in the following way. A circularly symmetric electron amplitude propagates from the STM tip into the surface state. It spreads radially outward until it gets scattered at a defect (an impurity or a step edge). A part of the amplitude is then back-reflected to the STM tip (scattering can even happen several times). Interference between the outgoing and back-reflected amplitude results in modulations of the LDOS, and thus the tunnelling current, as a function of position. The electron on the surface can be described by the following Hamiltonian $\widehat{H} = \widehat{H_0} + \widehat{V}$. $\widehat{H_0}$ is the Hamiltonian for the propagation into the surface state, while $\widehat{V}$ describes the potential perturbations due to impurities on the surface (in the case of the corral the impurities are the adatoms). Now, a relationship between the retarded Green's function $G^{\mathrm{ret}}(r',r,\varepsilon)$, the scattering eigenstates $\psi_\nu(r)$ of $\widehat{H}$ and the LDOS can be established:

$$\mathrm{LDOS}(r,\varepsilon) \equiv -\frac{1}{\pi}\mathrm{Im}[G^{\mathrm{ret}}(r,r',\varepsilon) = \sum_{\upsilon} |\psi_\upsilon(r)|^2 \delta(\varepsilon - E_\upsilon)$$

To determine the LDOS, a method for calculating the Green's function needs to be developed. The interested reader is referred to the publication by Fiete *et al* [110]. To simulate the standing wave patterns inside the corral, the phase shift occurring at the Fe adatoms needs again (as in the work by Crommie *et al* [48]) to be determined. For maximally absorbing Fe atoms, an excellent agreement between experiment and theory was obtained. This can be interpreted that the confinement of the surface state electrons by the corral is relatively poor because the Fe adatoms couple the surface state electrons strongly to the bulk states. The advantages of the scattering theory over the particle-in-a-box model are that (i) the eigenergies as well as the peak widths are generally well-described and (ii) the standing wave patterns of open structures can be predicted. On the other hand, within 7 Å of an adatom the scattering theory fails because the extra charge density of the adatom is not appropriately considered.

The multiple scattering theory was also used by Crampin *et al* [111] to describe the behaviour of surface state electrons in quantum corrals. They included the electron self-energy in their calculations and could demonstrate that this results in an improved agreement with the experiments. It is suggested that a key point in correctly reproducing all the experimental observations made, when studying quantum corrals with the STM, is to properly account for the observed leakage, i.e. to describe the underlying physics accurately. For example, Heller *et al* neglected—except the complex phase shift at the adatom boundary—other scattering channels. For this reason, the line widths and intensities of the peaks in STS spectra could not correctly be reproduced. However, despite the greatly improved agreement between experiment and theory when including the electron self-energy, the calculated lowest level width is still smaller. The theory by Crampin *et al* was later applied to describe the electron confinement in Mn atom arrays on Ag(1 1 1) [50] as well as to Ag nanoisland on Ag(1 1 1) [20]. Since it is not beforehand known what the relevant size of a nanoisland is—especially the effective boundary is important to model the confinement correctly—the results from the scattering theory were fitted with the energies obtained via the particle-in-a-box model. This implies that the effective boundary is a constant distance from the true atomic positions of the boundary.

To avoid specific assumptions or empirical input data, a different approach was taken by Niebergall *et al* [61]. They used *ab initio* calculations based on density functional theory and a multiple scattering approach employing the Korringa-Kohn-Rostocker Green's function method. As for the two approaches presented above: the crucial point lies in the determination of the Green's function to obtain a favourable agreement between experiment and theory. Nevertheless, the advantage of the *ab initio* approach is the start from one model without taking into account further assumptions. In this way, the surface state confinement in hexagonal vacancy islands on Cu(1 1 1) could be satisfactorily modelled. For this, the scattering at the vacancy boundary, which is formed by the monolayer high step of the vacancy island, is modelled by scattering at the adatoms of a corral having the same size as the vacancy island. The spatial modulation pattern of the LDOS as well as its amplitude and spectroscopic features are well reproduced. Even though electron–electron and electron–phonon interactions are not considered in the *ab initio* approach, while scattering of surface state electrons into bulk states are, the authors conclude (based on the favourable agreement between experiment and theory) that inelastic scattering is not the determining factor to explain the line width broadening of the states.

For describing the surface state confinement by pores made from molecular building blocks, the boundary element method (BEM) has been recently used [112] (see also the examples discussed in section 5). Primarily, the BEM has been extensively employed for solving Maxwell´s equation and determining the optical response for arbitrary shapes [113]. The calculations start with formulating the electromagnetic field scattered at the nanostructure as defined by the boundary charges and currents. The molecular pore is modelled via homogeneous regions of constant potential while the molecules are described by rectangles having an effective scattering potential. In the case of a metal-coordinated molecular network, a (different) potential is also assigned to the metal centres. The boundaries between the regions are assumed to be abrupt. The solution of the Schrödinger equation can then be given in terms of auxiliary electron boundary sources whose propagation is described with the electron Green's function. The calculated LDOS at different positions as well as conductance maps agree surprisingly well with the experimental data when taking into account that the model is rather simple. However, a limitation of the BEM approach is the fact that the scattering potential of the molecules (and metal centres) enters as an adjustable parameter in order to describe the experimental observations satisfactorily. Thus, the predictive power of this model is rather restricted.

5. Electron confinement in molecular porous networks

The first example of the confinement of the Shockley surface state by a honeycomb network prepared by molecular self-assembly was demonstrated by Lobo-Checa *et al* [114]. The network was prepared from the perylene derivative 4,9-diaminoperylene-quinone-3,10-diimine (DPDI) on the Cu(1 1 1) surface. Deposition of less than 0.7 ML (where 1 ML corresponds to the densest packed structure) at room temperature and subsequent annealing at 200 °C led to the formation of a well-ordered honeycomb network with a lattice constant of 2.55 nm, which can be described by a $p(10 \times 10)$ superstructure [115, 116] (see figure 1(a)). This extremely stable network is formed through a dehydrogenation of the amine and imine functional groups of the DPDI molecule (called 3deh-DPDI in the following) and subsequent metal coordination of the newly formed azo-groups to native Cu adatoms (see figure 1(b) for a tentative structure model).

STS spectra acquired at 5 K in the centre of a pore revealed a new occupied electronic state at −0.22 V while spectra taken on the clean Cu(1 1 1) surface just showed the characteristic steplike onset of the Shockley surface state at around −0.4 V (figure 1(d)). dI/dV maps recorded at the energy of the newly found electronic state at −0.22 V at the same area as the one shown in the topographic image in figure 1(a) revealed that this state is localized in the pores of the honeycomb network (figure 1(c)). Thus, it can be interpreted that each pore represents a single quantum dot within a regular 'quantum dot array' which confines the surface state electrons in all three dimensions. Complementary ARPES data taken for different coverages of the 3deh-DPDI network showed the appearance of a new weakly dispersing electronic band at 0.2 eV below the Fermi level. The spectrum in the top panel in figure 1(e) was acquired for a sample where in addition to the honeycomb network still bare metal areas were present. Both the Shockley surface state (red dashed line) and the new electronic state (black dashed line) can be discerned. For the sample completely covered with the 3deh-DPDI network (lowest panel in figure 1(e)), only the new electronic band is visible. Note that the white dashed lines in figure 1(e) indicate the surface Brillouin zone boundaries of the porous honeycomb network, which are separated by $|k_{\mathrm{parallel}}| = 0.142$ Å^{-1} what is one tenth of the Cu substrate periodicity and thus, in agreement with the LEED data. The existence of a weakly dispersing band can be explained by the coupling of neighbouring quantum dot states enabled through lossy scattering of the confined electrons at the boundaries of the pores. Similar forward scattering has been reported for complex systems like topological surface states of $Bi_{1-x}Sb_x$ [117] and for the spin-orbit split surface state of Bi thin films on Si(1 1 1) -7 × 7 [118]. Furthermore, the photoemission intensity present close to the Fermi level around the $\overline{M}$-point (best visible in the middle panel of figure 1(e)) can be attributed to the second subband, with its lowest energy at approximately 60 meV. A similar state can be seen in the STS spectra close to the Fermi level acquired in the centre of the pore (see figure 1(d)).

Soon after the first report on the confinement of surface state electrons by a metal-coordinated self-assembled honeycomb network, Klappenberger *et al* [119] and Krenner *et al* [25] demonstrated that the surface state electrons of Ag(1 1 1) can be confined by a hydrogen-bonded Kagomé lattice containing two different kinds of pores (having a triangular and a hexagonal shape) built from dicarbonitrile-sexiphenyl

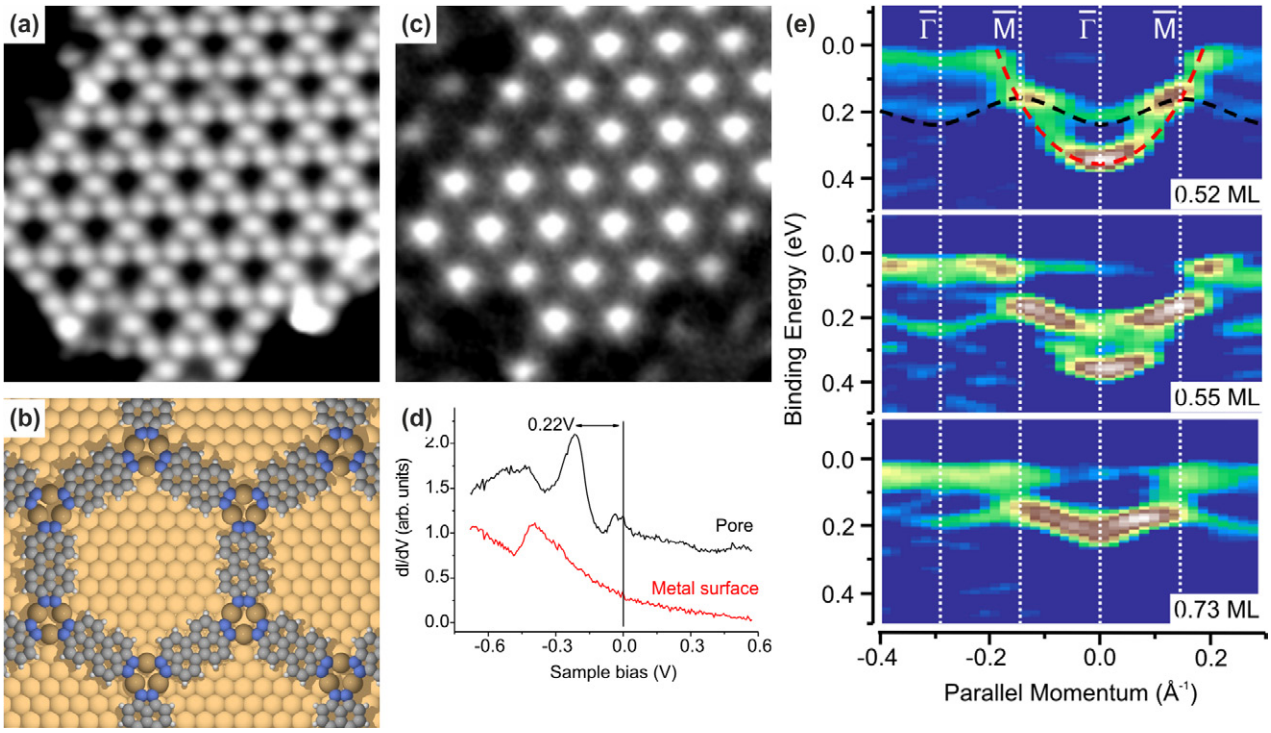

Figure 1. Electron confinement by a metal-coordinated molecular honeycomb network made from the perylene derivative 3deh-DPDI on Cu(1 1 1). (a) and (c) STM image and simultaneously recorded d*I*/d*V* map at −0.22 V (13.6 nm × 13.6 nm). (b) Tentative structure model of the metal-coordinated porous network. (d) d*I*/d*V* spectra measured inside a pore (black line) and on the clean Cu surface far away from the porous network (red line). (e) ARPES data measured along the $\overline{\Gamma}\overline{M}$-direction for the porous network at different coverages. By using the second derivative, an enhancement of the features of the energy dispersion curves was obtained. The white dashed lines indicate the high symmetry points of the superstructure Brillouin zone while the black and red dashed lines in the top panel indicate the weakly dispersing band of the confined state and the parabolic Shockley surface state of the clean Cu(1 1 1) surface, respectively. The spectrum shown in the central panel for 0.55 ML was taken at 60 K while the other two spectra were acquired at room temperature. Adapted with permission from [114, 115].

(NC-Ph$_6$-CN) molecules. Similar to earlier reports on the confinement of surface state electrons, the lowest lying state confined in the smaller triangular pores was found at higher energies (60 mV) than the lowest lying state confined in the larger hexagonal pores (−20 mV) (see figures 2(a) and (b)). d*I*/d*V* maps taken at different energies exhibit chirality for the LDOS, which derives from the chiral Kagomé lattice. To compare the differential conductance in the triangular and the hexagonal pore, d*I*/d*V* spectra were taken along the green line drawn in figure 2(d). It becomes evident that the onset of the lowest lying state around −10 mV is in the centre of the large hexagonal pore. Between 50 mV and 200 mV, the second eigenstate appears having its maximum intensity half way between the pore centre and the molecules forming the hexagonal pore (see figure 2(b), red curve). At even higher energies, three maxima are visible. On the other hand, the triangular pores show a very broad resonance between −50 mV and 200 mV. At higher energies, additional features can be observed in the triangular pores. Above 300 mV, the resonance is split into two maxima. Additionally, the spectra in the two triangular pores—right and left of the hexagonal pore—exhibit a slightly different appearance due to the asymmetry of the triangles with respect to the scan line.

Calculations with the BEM, where the Schrödinger equation is solved for a planar surface patterned by rectangular areas of constant scattering potential of 500 meV to mimic the molecules, gave very similar point spectra (bias voltage position and relative intensity) as observed experimentally (figures 2(b) and (c)). Further calculations were conducted for triangles having one, two or three neighbouring triangles to investigate the interaction of neighbouring pores on the LDOS. No significant differences were found for the increasing number of neighbouring pores. This indicates that the interaction between neighbouring pores is rather weak and plays (almost) no role in the formation of the standing wave patterns.

The same dicarbonitrile-oligophenyl (NC-Ph$_n$-CN) linkers containing either four or six phenyl rings were used to prepare a cobalt-coordinated molecular honeycomb network on Ag(1 1 1). For both networks the confinement of the surface state electrons inside the hexagonal pores was reported (figures 3(a)–(c)) [120]. It was shown that the lowest lying electronic state strongly depends on the size of the pores. While the energy for this state was found close to the Fermi level for the network formed by NC-Ph$_6$-CN, it was shifted above the Fermi level into the unoccupied states for the smaller NC-Ph$_4$-CN network. The STS spectra taken at different positions within the pores, in the centre of the molecule and on the Co atom for the network made from NC-Ph$_6$-CN show significantly different characteristics (figure 3(c)). In the centre of the pore (black line in figure 3(c)), two clear maxima corresponding to the first and fourth eigenstates as well as two shoulders on either side of the second maximum can be identified. The spectrum

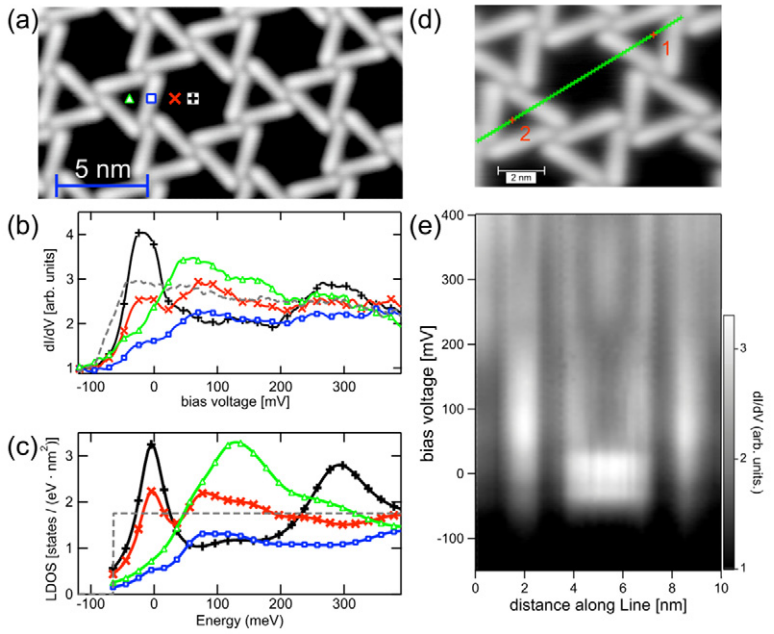

Figure 2. Confinement of the Ag(1 1 1) Shockley surface state by a hydrogen-bonded Kagomé lattice made from dicarbonitrile-sexiphenyl molecules. (a) STM image of the Kagomé lattice. The coloured symbols represent the positions at which the d*I*/d*V* spectra displayed in (b) where recorded. (c) Theoretical d*I*/d*V* spectra simulated with BEM at the positions marked in (a). (d) STM image showing the line along which the d*I*/d*V* spectra displayed in (e) as a plot of the differential conductivity were recorded. Adapted with permission from [119].

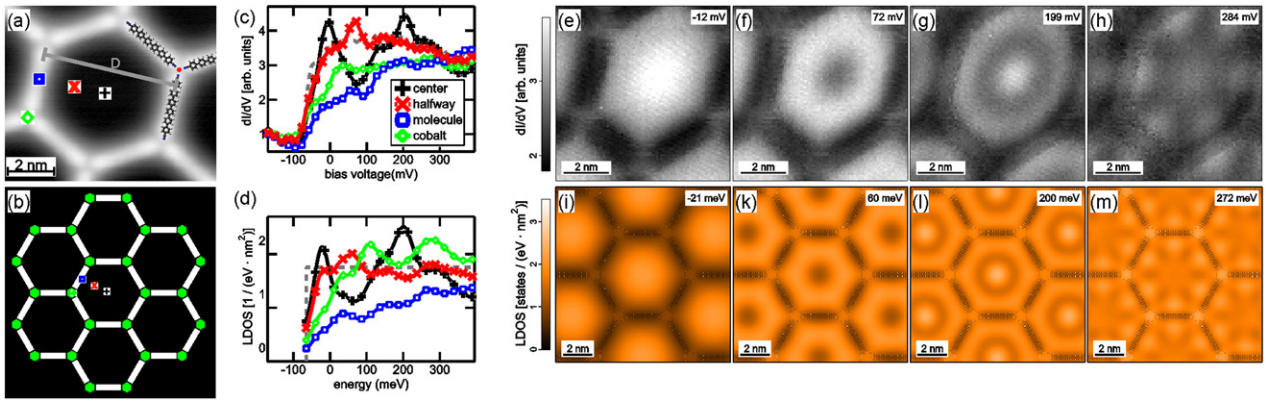

Figure 3. Surface state confinement in a metal-coordinated honeycomb network made from dicarbonitrile-sexiphenyl molecules and Co atoms on Ag(1 1 1). (a) STM image of a single pore. The coloured symbols indicate the positions where the d*I*/d*V* spectra shown in (c) were acquired. (b) 2D potential model used in the BEM calculations. (d) Conductance spectra calculated with the BEM. (e)–(h) Measured d*I*/d*V* maps at the indicated biases corresponding to the first, second, fourth and fifth energy eigenstate and (i)–(m) corresponding calculated LDOS. Adapted with permission from [120].

taken halfway between the centre of the pore and a molecule (red line in figure 3(c)) displays one prominent peak around 68 mV. This can be related to the second eigenstate, which shows a minimum in the centre of the pore. In contrast, the spectra taken on the molecule or on the Co atom do not show any pronounced peaks (blue and green line, respectively).

To investigate the spatial distribution of the LDOS, d*I*/d*V* maps were taken at different bias voltages (figures 3(e)–(h)). Figures 3(e) and (f) display the first and second eigenstate while the d*I*/d*V* map taken at 200 mV (figure 3(g)) resembles a mixture of the third and fourth eigenstates, which cannot be resolved because of the width of the resonances. The map shown in figure 3(h) is equal to the distribution of the fifth eigenstate. The calculation of the eigenstate energies E_N can be approximately done by numerically analysing the confinement of a particle in a 2D hexagonal box. Accordingly, the eigenenergies can be calculated by the following formula: $E_N = E_0 + \frac{\lambda_n}{m^* A}$ with $A = \cos\left(\frac{\pi}{6}\right) D^2$ being the area of the hexagonal pore with the width D as described in figure 3(a), m* being the reduced mass of the electron and λ_n being the *n*th eigenvalue. The calculated values fit very well with the experimentally obtained ones when using an effective pore size of $D_{eff} = 1.05$ D. The requirement of an effective pore size, which is larger than the real pore size, indicates a substantial penetration of the electron wave functions of one pore

into neighbouring pores. Simulations using the BEM gave additional information on the confinement properties of the honeycomb network. Similar to the BEM simulations carried out for the Kagomé lattice (*vide supra*), an effective scattering potential of 500 meV was used for the molecules and a potential of −50 meV was assumed for the hexagonal Co regions (see figure 3(b)). This can be interpreted that electron scattering is repulsive for the molecules and slightly attractive in the case of the Co coordination centres. The calculated spectra (figure 3(d)) and the electron wave patterns (figures (i)–(m)) generally agree very well with the measured data, despite the simplicity of this model. Only at the Co sites, differences are found for energies higher than 100 mV. In the simulated d*I*/d*V* maps a significant contribution of the Co atoms to the density of states can be seen, which is not present in the experimental d*I*/d*V* maps (figures 3(g), (h) and (l), (m)). This effect is also visible in the density of states spectra were the intensity measured on the Co atom is significantly lower than the one in the calculated spectra (figures 3(c) and (d)).

A study comparing the dependence of the surface state confinement by three isostructural metal-coordinated honeycomb networks on Cu(1 1 1) constructed from three different molecules and thus, exhibiting different unit cell sizes was performed by Wang *et al* [121]. 1,3,5-tris(pyridyl)benzene (M1), 1,3,5-tris[4-(pyridin-4-yl)phenyl]benzene (M2) and 1,3,5-tris(4-bromophenyl)benzene (M3) (see inset in figures 4(a)–(c)) were used to create the Cu-coordinated honeycomb networks. After annealing at 120 °C, for all molecules the formation of a metal-coordinated network with native Cu adatoms is observed. While M1 and M2 both contain pyridyl functional groups and only differ in size, M1 and M3 have approximately the same size but M3 possesses Br-functionalized endgroups. Thus, M3 forms a proto-polymer by splitting off the Br atoms upon annealing and undergoing strong C–Cu–C bonding. d*I*/d*V* spectra recorded in the pore centre for each of the porous honeycomb networks exhibit one relatively broad peak in the occupied states region. The width of the peak was explained by imperfect confinement (figure 4(f)). The peak positions were found to strongly depend on the pore size as well as on the functional groups of the molecules. For the network created by the M2 molecules, a peak at higher binding energy was observed compared to the networks created from M1 and M3 molecules. This is expected as the M2 network exhibits a larger unit cell size as well as larger pores, which leads to a confined state energy closer to the one of the pristine surface state. The M3 network exhibits a peak at lower binding energy than the one of the M1 network, although the pore and unit cell sizes are comparable. This indicates a different scattering potential for the two networks. Furthermore, for each of the three networks, slight differences in the peak position, shape and intensity were observed for different pores. This was also confirmed by d*I*/d*V* maps, which demonstrate that the LDOS intensity is not equally distributed over the different pores.

The band dispersions of the confined states reported in figures 4(d) and (e) were obtained by Fourier transformation of the d*I*/d*V* maps measured at different energies for the honeycomb networks created by both M1 and M2 molecules. For the M3 network this was not possible because the island sizes

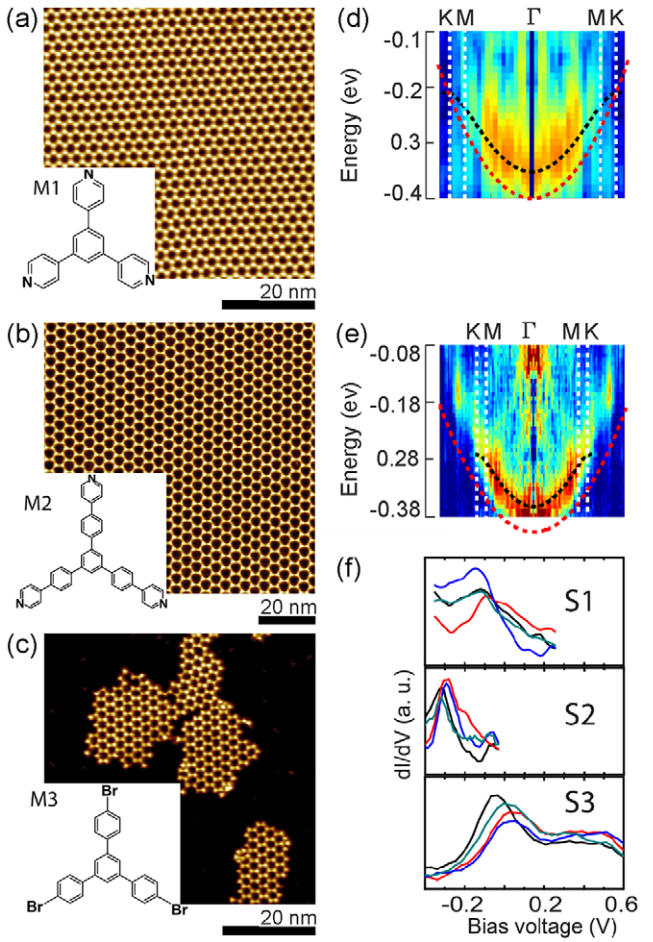

Figure 4. Metal-coordinated networks formed from (a) M1, (b) M2 and (c) M3 molecules (the insets show the molecular structure) on Cu(1 1 1). (d) and (e) Power spectral functions of the 2D electron gas formed from the M1 and M2 networks, respectively. The red dashed curves indicate the surface state dispersion of the clean Cu(1 1 1) surface, the black dashed lines highlight the simulated first order bands and the white dashed lines indicate high symmetry points of the molecular Brillouin zones. (f) d*I*/d*V* spectra recorded at the centre of the pores formed by M1 (top), M2 (middle) and M3 (bottom) molecules. Adapted with permission from [121].

were too small. Both networks show a dispersive band in the first Brillouin zone (indicated by the white dashed lines in figures 4(d) and (e)) whereas the intensity close to the Brillouin zone boundaries is strongly reduced. The black dotted curves in figures 4(d) and (e) represent the calculated first band by using a DFT total potential in which the effective potential of the molecules is 300 meV and −100 meV for the Cu adatoms. Noteworthy, the dispersion for the M1 (120 meV) and M2 network (110 meV) slightly exceeds the one reported for the 3deh-DPDI network (80 meV), which was measured by ARPES (see figure 1(e)). The reason might be a difference in the lossy scattering and imperfect confinement in the different cases.

Recently, a 2D porous sponge-like network was prepared on a Cu(1 1 1) surface through on-surface covalent coupling of a perylene derivative containing two borylene functional groups with trimesic acid (TMA) [122]. These pores exhibit several different geometrical shapes and sizes as visible in figure 5(a), what makes them good candidates to study the

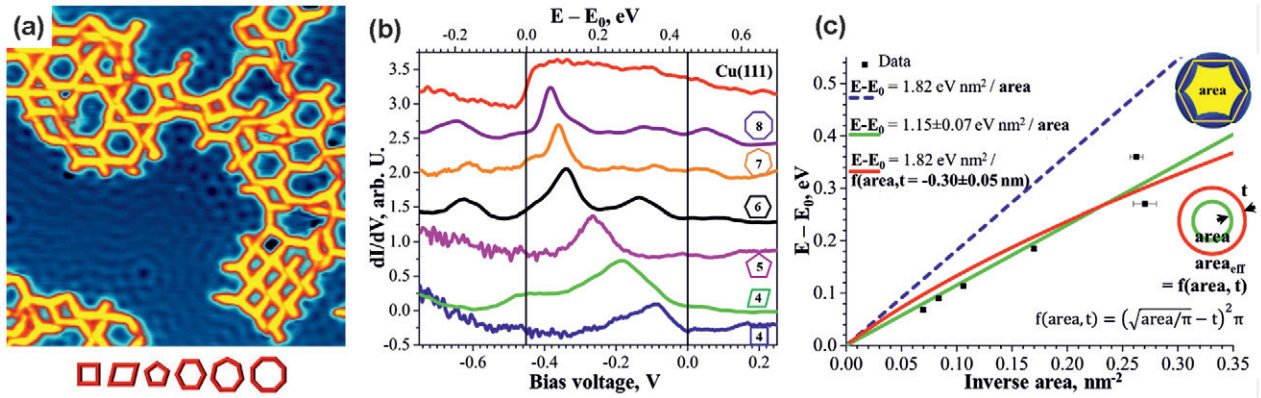

Figure 5. Covalently coupled molecular network formed from TMA and a borylene-functionalized perylene derivative on Cu(1 1 1). (a) STM image (30 nm × 30 nm) showing pores with different sizes and shapes. Sketches of the different pore sizes and shapes observed are displayed below the STM image. (b) d*I*/d*V* spectra taken in the centre of the different pores (indicated by symbols next to the spectra) and on the clean Cu(1 1 1) surface (red spectrum). (c) Plot of the energy of the confined state with respect to the onset energy of the pristine surface state as a function of the inverse pore area. The red and green lines are based on calculations for different effective pore areas (see text). Adapted with permission from [122].

dependence of the surface state confinement on the geometry and size of the confining cavity. STS spectra taken in the centre of different pores showed that the energies of the confined states shifted towards the Fermi level with decreasing pore size (figure 5(b)). The energy of the confined state can be calculated by $E = E_0 + \frac{\alpha_1 \hbar^2 \pi}{2m^* A}$, where A is the pore area, α_1 is a shape dependent parameter [123] and E_0 is the onset of the native surface state. In figure 5(c) E–E_0 is plotted with respect to the inverse pore area for the experimental (green line indicates the fit) and the calculated data (red and blue line). For the blue line, a circular confinement was assumed. However, it is clearly visible that the slope of the fit for the measured data deviates significantly from the calculated one. By introducing a fit parameter $f(\text{area}, t) = (\sqrt{\text{area}/\pi} - t)^2 \pi$ to describe the effective area correctly, which confines the surface state electrons, a reasonably good agreement can be obtained for $t = 0.3$ nm between measured and calculated data (red line). This indicates that the effective pore diameter is 0.3 nm larger than the one derived by using the centre of the molecules as the boundaries of the pore. This finding is similar to what was described for the porous network formed from Co-coordinated NC-Ph$_6$-CN molecules on Ag(1 1 1) (*vide supra*) [120]. Shchyrba *et al* could also demonstrate that upon partial confinement, i.e. if one or two sides of a hexagonal pore are missing, the surface state is still confined and the energy of the lowest lying state does not change compared to the one of a closed pore of similar size. The only difference is that the peak is considerably broadened, probably due to incomplete confinement and interference of the confined and the free electrons of the surface state.

Except for the investigation of the surface state confinement by the 3deh-DPDI network on Cu(1 1 1) (the first example presented in this chapter), where a combination of STS and ARPES was used, only STS and/or d*I*/d*V* mapping has so far been employed to study the confining properties of molecular porous networks on (1 1 1)-oriented noble metal surfaces. One of the main reasons is the requirement that only one well-ordered molecular phase should homogeneously cover the sample surface in order to obtain conclusive results from a laterally averaging technique like ARPES. However, that is in many cases difficult to obtain. Moreover, the irradiation with UV light as well as the emission of photoelectrons in the case of ARPES can lead to beam damage and consequently, the samples often deteriorate quickly before they can be studied in detail. In contrast, the unique possibility of STS to locally study occupied as well as unoccupied states makes it the preferred technique to investigate the confinement of surface state electrons by porous molecular networks. By acquiring d*I*/d*V* maps over a large energy range and performing Fourier transformation, the energy dispersion relation of the confined states can be addressed as it was for example shown by Wang *et al* (see figure 4) [121].

In the following, we would like to provide a qualitative comparison of the confinement properties of the porous molecular networks discussed above. From the experimental results it can be concluded that the smaller the pore size the larger the shift of the confined state towards lower binding energies [119–122]. In addition, when comparing the available reports one may arrive at the conclusion that the intermolecular interactions holding together the various porous molecular networks influence the confining properties in such a way that for stronger intermolecular interactions the confinement is stronger, i.e. the shift of the confined state compared to the pristine surface state is larger. However, a quantitative comparison of the confinement properties of the different molecular networks is more complicated. For example, the molecule-substrate interactions as well as the width of the molecular building blocks representing the width of the confinement barrier should be taken into account. The fact that a larger pore size than the actual one had to be assumed when using the particle in the box model to approximately calculate the position of the confined state [122] hints at the influence of the second consideration. Moreover, we suggest that additional investigations of the confinement effects of porous molecular networks adsorbed on Au(1 1 1) will help to shed light onto the influence of the substrate.

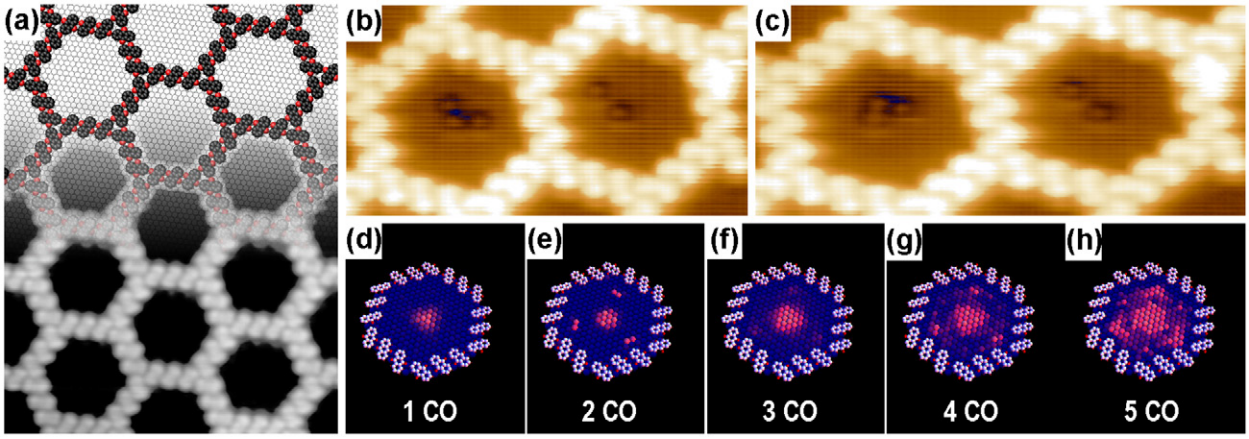

Figure 6. Confinement of CO molecules in an anthraquinone network adsorbed on Cu(1 1 1). (a) Molecular network formed by anthraquinone on Cu(1 1 1). Three molecules form one side of the pore. The upper part shows the molecular model and the lower part the STM image (15 nm × 26 nm). (b) and (c) STM images taken from a movie showing the rearrangement of CO molecules in the pores. (d)–(h) Probability of the CO occupation inside an anthraquinone pore for different CO occupancies. Adapted with permission from [124, 126].

6. Confinement of adsorbates in molecular porous honeycomb networks

As described in the introduction, the surface state of free metal surfaces can strongly influence the self-assembly of adsorbates [33–38, 43–46]. In the following, three examples are presented on how the surface state confined in the pores of honeycomb networks influences the self-assembly of guest atoms or molecules in the pores. As a first example, the confinement of CO molecules in a honeycomb network made from anthraquinone molecules on Cu(1 1 1) is discussed. The formation of this hydrogen-bonded network was explained by the confinement of the surface state electrons in the hexagonal pores [124, 125]. Each side of the pore consists of three parallel molecules and has a diameter of approx. 4 nm (see figure 6(a)), which is several times larger than the size of one molecule. The formation of this regular pattern—although pores with two or four molecules per side would be in principle possible—was explained by the creation of a noble gas configuration (i.e. two filled shells) when the surface state electrons of Cu(1 1 1) are confined within these pores. Calculations showed that pores with a different number of molecules per side would not exhibit this noble gas configuration.

For low coverage, CO was found to preferentially adsorb in the centre of the anthraquinone pores (figure 6(d)), i.e. at the high electron density areas. No diffusion of the CO molecules between the pores was observed meaning that CO is confined to one pore (figures 6(b) and (c)) [126]. However, diffusion inside the pore was detected (see the consecutively taken STM images in figures 6(b) and (c)). Figures 6(d)–(h) show colour-coded histograms for the probability of occupation in one pore depending on the amount of CO molecules in the pore. The probability to find a CO molecule in one of the two innermost possible adsorption sites amounts to 54%. For two molecules, either both occupy the central area or one is located in the centre while the second CO molecule is found at one of three equivalent adsorption sites halfway towards one of the vertices of the hexagonal pore. Similar adsorption sites are favoured for higher CO coverages up to five molecules. The fact that a threefold symmetry was found for the preferred adsorption positions can be explained by the threefold symmetry of the adsorbed honeycomb network (the vertices are alternatingly centred on fcc and hcp sites). For even higher CO coverage, the molecules form a $(\sqrt{3} \times \sqrt{3})$ R30° structure similar to CO adsorbed on a clean Cu(1 1 1) surface [127–129]. However, due to the limited number of adsorption sites inside the pore dislocation lines are often found, which seems to be energetically more favourable than leaving adsorption sites close to the boundaries of the pores free [130]. These dislocation lines show considerable mobility, which leads to a constant change in their position and geometry. For slightly lower coverages, CO vacancies are found inside the pores, which show a much higher diffusion compared to the clean Cu(1 1 1) surface. Furthermore, the vacancies are confined to the edges of the pores while the chances to find vacancies in the centre of the pores are considerably lower.

Recently, the adsorption of Fe atoms was investigated inside the pores of a honeycomb network formed by coordination of NC-Ph_5-CN molecules to native Cu adatoms on Cu(1 1 1) [131]. Deposition of small amounts of Fe at 12 K led to pores filled with 0, 1, 2, 3 and 4 Fe atoms (figure 7(a)) whereas the filling followed a binomial distribution. For more than one Fe atom in the pore, preferred interatomic distances were observed, which are comparable to the spacing between Fe atoms on bare Cu(1 1 1) and which originate from long-range oscillatory interactions caused by the Cu surface state electrons. Single Fe atoms—as well as the centre of mass for dimers and trimers—are found in the centre of the pore (figures 7(b)–(d)). The atomic distances for dimers and trimers are the same (1.1 nm) while there is no (an) adsorption site preference for the dimers (trimers). This triangular distribution observed for the trimers (figure 7(c)) can be explained by the threefold symmetry of the porous network arising from the asymmetry of every second threefold metal-coordinated vertex. Slight annealing to 18 K led to the formation of clusters (consisting of 2, 3, or 4 atoms as evidenced by their apparent height), which appear as single objects inside the pores while the number of empty pores stayed the same. This indicates

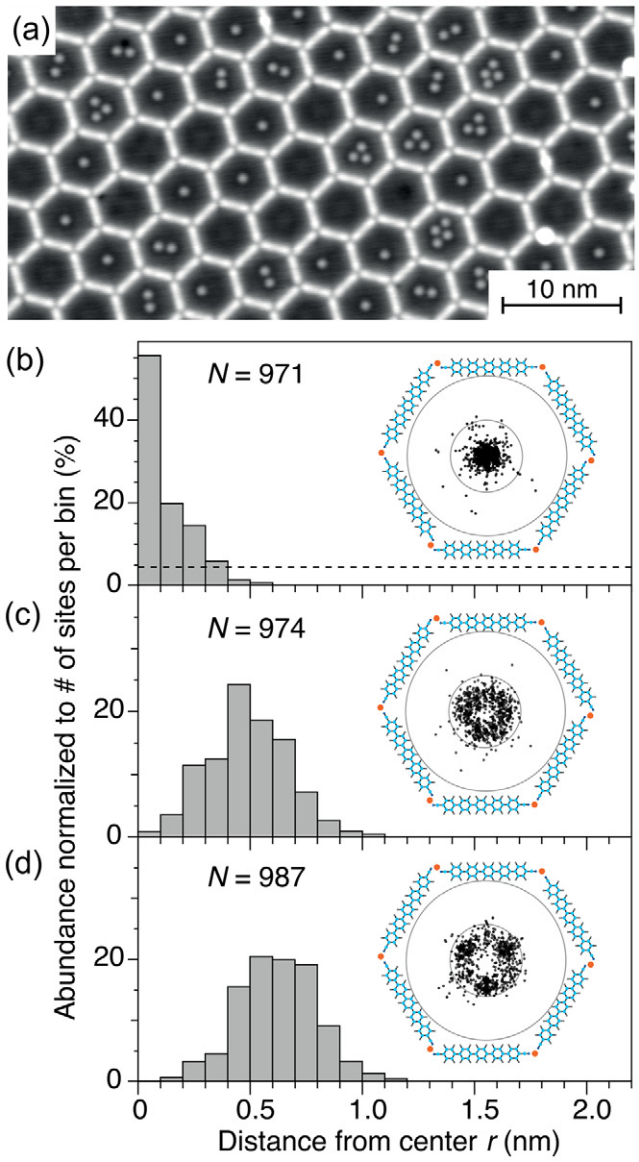

Figure 7. Honeycomb network formed from dicarbonitrile pentaphenyl molecules and Cu adatoms on Cu(1 1 1) and subsequently filled with Fe atoms. (a) STM image of the network. Different numbers of Fe atoms trapped inside the pores are visible. (b)–(d) Adsorption site statistics for the Fe adatoms trapped in the network pores for occupancies of one (b), two (c) and three (d) Fe atoms. Adapted with permission from [131].

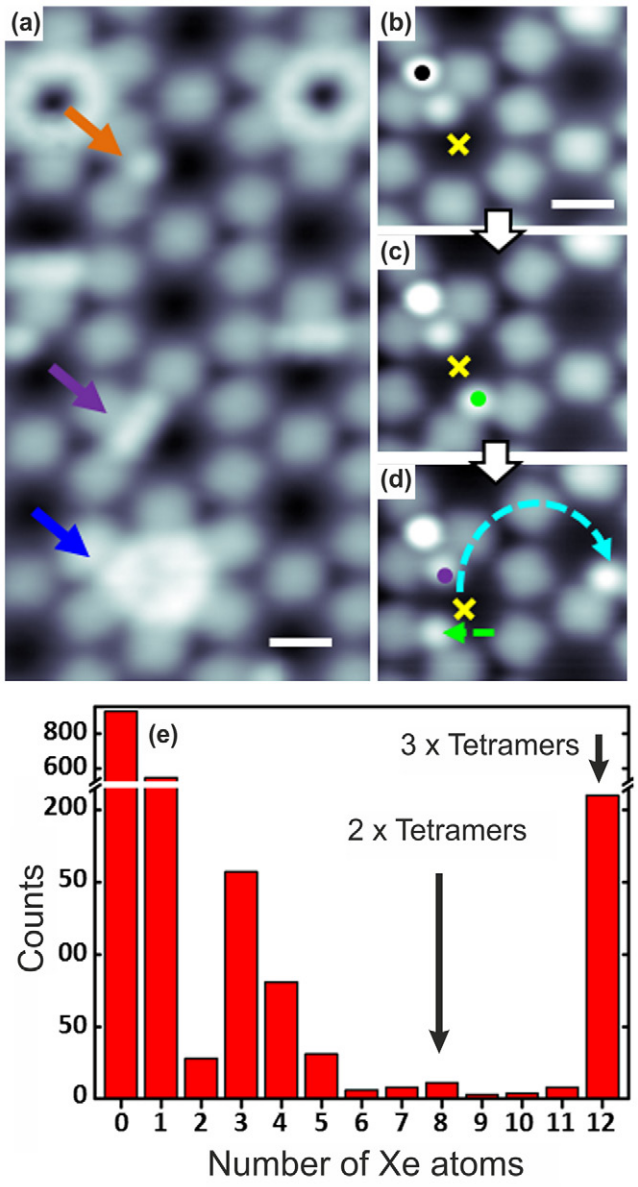

Figure 8. Xe adsorbed in the pores of the 3deh-DPDI network on Cu(1 1 1). (a) STM image from which different Xe occupancies in the pores can be discerned: a pore containing a single atom (orange arrow), a partially filled pore (violet arrow) and a completely filled pore with 12 Xe atoms (blue arrow) are visible. (b)–(d) Atom manipulation of single Xe atoms to controllably increase the number of Xe atoms per pore one by one. The Xe-decorated tip was placed above the centre of the pore marked with the yellow cross. Upon placing the Xe atom from the tip into the pore (c), it migrated to the boundary of the pore (green dot). In the following attempt (d), one atom jumped into the neighbouring pore (blue dashed arrow) and the other one moved to a different place (green arrow). The observed behaviour is indicative of repulsion between Xe and the confined state. (e) Histogram of Xe occupancy in the pores of the 3deh-DPDI network. The behaviour clearly deviates from a Poisson distribution. All scale bars: 1 nm. Adapted with permission from [132].

that no Fe atom diffusion from one pore to another happened. Also the binomial distribution of the occupation of the pores stayed unaltered.

The atom-by-atom condensation of xenon in well-defined 'quantum boxes' fabricated from 3deh-DPDI molecules on Cu(1 1 1) (see figure 1) was recently investigated by Nowakowska *et al* [132]. In contrast to CO molecules or Fe atoms, whose self-assembly was previously investigated in other porous networks (*vide supra*), xenon atoms exhibit a closed-shell structure and thus, can only undergo weak van der Waals interactions. Xe was never found in the centre of the pore what is explained by Pauli repulsion between Xe and the ground state of the confined surface state. This behaviour was corroborated by repositioning experiments in which individual Xe atoms were tried to be placed in the centre of the pore what only resulted in the presence of Xe at the periphery of the pore or in hopping of the Xe atom into a neighbouring pore (figures 8(b)–(d)). On the other hand, CO molecules as well as Fe atoms were found to attractively interact with the

Cu surface state confined in different honeycomb networks. The histogram of the spontaneously occurring occupancies (figure 8(e)) indicates that the presence of certain numbers of Xe atoms in the pores is preferred with the highest probability for one and twelve atoms and an additional preference for three and eight atoms. This is in contrast to the Poison distribution, which was found for the occupancy of Fe atoms in the NC-Ph_5-CN network. A detailed analysis of the different observed occupancies **occ-n** was carried out under the aspect whether **occ-n** is equal to **occ-(n-1)** plus one additional Xe atom or whether **occ-n** can be described by the superposition of two structures present for lower occupancies. The observed occupancies cannot be described by a single set of hierarchic filling rules. Instead, the interplay of different weak forces (interatomic forces between Xe atoms, interaction between Xe and the confined state as well as with the molecules) determines the observed filling levels of the pores.

7. Conclusion and outlook

The fascinating achievement to confine the surface state electrons to corrals made from Fe adatoms on Cu(1 1 1) and to visualize the electronic structure of this confinement inspired researchers over the last two decades to experimentally as well as theoretically study the interplay of metal surface states with low-dimensional atomic and molecular structures. Especially the advent of the STM enabled such experimental studies and attracted a lot of research interest. Replacing adatoms by molecular building blocks for the construction of porous nanostructures to confine metal surface states offers several advantages. Molecular self-assembly, which is normally used to fabricate the porous networks, is a parallel process and thus, produces billions of pores at the same time. The process itself is fast compared to the time-consuming atom manipulation with the STM tip used for the construction of corrals from adatoms. Furthermore, for well-ordered molecular honeycomb networks the influence of the confined states of neighbouring pores on each other can be examined.

So far, mainly with STS and taking dI/dV (conductance) maps the electronic states confined to the molecular pores were analysed. It has been already found—similar to what has been reported for corrals made from adatoms—that the energy of the confined state generally depends on the area of the confining pore when the same class of molecules is used. However, one study done with different molecules but very similar size reported a deviation of this behaviour. This asks for further investigations (experimentally as well as theoretically) comparing the influence of the molecular backbone as well as the intermolecular interactions stabilizing the porous networks on the confined state. Differences with respect to the scattering and absorption behaviour of the molecules are expected which then lead to different eigenenergies for similar sized pores fabricated from different molecules.

Up to now, there is only one report available which experimentally investigated the interaction of neighbouring confined states. For 3deh-DPDI on Cu(1 1 1) the coupling of the confined states enabled through so-called lossy scattering resulted in the formation of a 2D band structure. This means by patterning metal surfaces with porous molecular networks a uniform change of the electronic surface properties may be achieved. This possibility should also attract interest in catalysis research or prospective (nano)electronics applications.

The pores can be also used to study the adsorption of guest entities and their interaction with the confined state. So far, mainly atoms and diatomic molecules were used. The influence of the confined state onto these guests became evident because favourable and unfavourable adsorption sites were observed due to attractive and repulsive interactions of the guests with the confined state. The question is how larger molecules will be influenced by the confined state and if they are similarly affected by it. However, it is not only the adsorption of guest entities, which is changed in comparison to adsorption on a pristine surface, but also the reaction conditions inside the pore should be affected. This asks for studies of basic chemical reactions inside the pores whose outcome and pathway are well-understood on the pristine metal surfaces.

In conclusion, the field for further experimental and theoretical studies of confinement phenomena with molecular porous networks is wide open and exciting as well as surprising results can be expected.

Acknowledgments

This work was supported by the Foundation for Fundamental Research on Matter (FOM), part of the Netherlands Organisation for Scientific Research (NWO), by the European Research Council (ERC-2012-StG 307760-SURFPRO) and by NWO (Chemical Sciences, VIDI-grant No. 700.10.424 and VENI-grant No. 722.012.010). We would like to thank all current and former team members and project partners co-authoring cited joint publications.

References

[1] Hasan M Z and Moore J E 2011 3D topological insulators *Annu. Rev. Condens. Matter Phys.* **2** 55–78
[2] Roduner E 2006 Size matters: why nanomaterials are different *Chem. Soc. Rev.* **35** 583–92
[3] Jortner J 1992 Cluster size effects *Z. Phys.* D **24** 247–75
[4] Shockley W 1939 On the surface states associated with a periodic potential *Phys. Rev.* **56** 317–23
[5] Tamm I 1932 On the possible bound states of electrons on a crystal surface *Phys. Z. Soviet Union* **1** 733
[6] Bertel E 1995 1 and 2D surface states on metals *Surf. Sci.* **331–3** 1136–46
[7] Braun J 1996 The theory of angle-resolved ultraviolet photoemission and its applications to ordered materials *Rep. Prog. Phys.* **59** 1267–338
[8] Goldman A, Dose V and Borstel G 1985 Empty electronic states at the (1 0 0), (1 1 0), and (1 1 1) surfaces of nickel, copper, and silver *Phys. Rev.* B **32** 1971–80
[9] Heimann P, Neddermeyer H and Roloff H F 1973 Ultraviolet photoemission for intrinsic surface states of the noble metals *J. Phys. C: Solid State Phys.* **10** L17–22
[10] Kevan S D and Gaylord R H 1987 High-resolution photoemission study of the electronic structure of the noble-metal (1 1 1) surfaces *Phys. Rev.* B **36** 5809–18

[11] Paniago R, Matzdorf R, Meister G and Goldmann A 1995 Temperature dependence of shockley-type surface energy bands on Cu(1 1 1), Ag(1 1 1) and Au(1 1 1) *Surf. Sci.* **336** 113–22

[12] Reinert F and Nicolay G 2004 Influence of the herringbone reconstruction on the surface electronic structure of Au(1 1 1) *Appl. Phys.* A **78** 817–21

[13] Smith N V and Woodruff D P 1986 Inverse photoemission from metal surfaces *Prog. Surf. Sci.* **21** 295–370

[14] Wern H, Leschik G, Hau U and Courths R 1984 Band structure of Ag, Au and Pt along the Δ line near *X* from angle resolved photoemission spectroscopy (ARUPS): Location of transitions via evanescent gap surface states *Solid State Commun.* **50** 581–6

[15] Crommie M F, Lutz C P and Eigler D M 1993 Imaging standing waves in a 2D electron gas *Nature* **363** 524–7

[16] Gross L, Moresco F, Savio L, Gourdon A, Joachim C and Rieder K-H 2004 Scattering of surface state electrons at large organic molecules *Phys. Rev. Lett.* **93** 056103

[17] Hasegawa Y and Avouris P H 1993 Direct observation of standing wave formation at surface steps using scanning tunneling spectroscopy *Phys. Rev. Lett.* **71** 1071–4

[18] Petersen L, Sprunger P T, Hofmann P H, Lægsgaard E, Besenbaceher F and Plummer E W 1998 Direct imagining of the 2D Fermi contour: fourier-transform STM *Phys. Rev.* B **57** R6858–61

[19] Jeandupeux O, Bürgi L, Hirstein A, Brune H and Kern K 1999 Thermal damping of quantum interference patterns of surface-state electrons *Phys. Rev.* B **59** 15926–34

[20] Li J, Schneider W-D, Berndt R and Crampin S 1998 Electron confinement to nanoscale Ag islands on Ag(1 1 1): a quantitative study *Phys. Rev. Lett.* **80** 3332–5

[21] Li J, Schneider W-D and Berndt R 1997 Local density of states from spectroscopic scanning-tunneling-microscopy *Phys. Rev.* B **56** 7656–9

[22] Hörmandinger G 1994 Imaging of the Cu(1 1 1) surface state in scanning tunneling microscopy *Phys. Rev.* B **49** 13897–905

[23] Wagner C, Franke R and Fritz T 2007 Evaluation of I(V) curves in scanning tunneling spectroscopy of organic nanolayers *Phys. Rev.* B **75** 035421

[24] Ziegler M, Néel N, Sperl A, Kröger J and Berndt R 2009 Local density of states from constant-cutter nt tunneling spectra *Phys. Rev.* B **80** 125402

[25] Krenner W, Kühne D, Klappenberger F and Barth J V 2013 Assessment of scanning tunneling spectroscopy modes inspecting electron confinement in surface-confined supramolecular networks *Sci. Rep.* **3** 1454

[26] Nicoara N, Román E, Gómez-Rodríguez J M, Martín-Gago J A and Méndez J 2006 Scanning tunneling and photoemission spectroscopies at the PTCDA/Au(1 1 1) interface *Org. Electron.* **7** 287–94

[27] Scheybal A, Müller K, Bertschinger R, Wahl M, Bendounan A, Aebi P and Jung T A 2009 Modification of the Cu(1 1 0) Shockley surface state by an adsorbed pentacene monolayer *Phys. Rev.* B **79** 115406

[28] Schwalb C H, Sachs S, Marks M, Schöll A, Reinert F, Umbach E and Höfer U 2008 Electron lifetime in a Shockley-type metal-organic interface state *Phys. Rev. Lett.* **101** 146801

[29] Ziroff J, Gold P, Bendounan A, Forster F and Reinert F 2009 Adsorption energy and geometry of physisorbed organic molecules on Au(1 1 1) probed by surface-state photoemission *Surf. Sci.* **603** 354–8

[30] Bischler U and Bertel E 1993 1D surface states (chain states) on a metal surface: H on Ni(1 1 0) *Phys. Rev. Lett.* **71** 2296–9

[31] Lindgren S Å, Paul J and Walldén L 1982 Surface state energy shifts by molecular adsorption: CO on clean and Na covered Cu(1 1 1) *Surf. Sci.* **117** 426–33

[32] Moore A M and Weiss P S 2008 Functional and spectroscopic measurements with scanning tunneling microscopy *Annu. Rev. Anal. Chem.* **1** 857–82

[33] Han P and Weiss P S 2012 Electronic substrate-mediated interactions *Surf. Sci. Rep.* **67** 19–81

[34] Ding H F, Stepanyuk V S, Igenatiev P A, Negulyaev N N, Niebergall L, Wasniowska M, Gao C L, Bruno P and Kirschner J 2007 Self-organized long-period adatom strings on stepped metal surfaces: scanning tunneling microscopy, *ab initio* calculations and kinetic Monte Carlo simulation *Phys. Rev.* B **76** 033409

[35] Knorr N, Brune H, Epple M, Hirstein A, Schneider M A and Kern K 2002 Long-range adsorbate interactions mediated by a 2D electron gas *Phys. Rev.* B **65** 115420

[36] Repp J, Moresco F, Meyer G and Rieder K-H 2000 Substrate mediated long-range oscillatory interaction between adatoms: Cu/Cu(1 1 1) *Phys. Rev. Lett.* **85** 2981–4

[37] Silly F, Pivetta M, Ternes M, Patthey F, Pelz J P and Schneider W-D 2004 Creation of an atomic superlattice by immersing metallic adatoms in a 2D electron sea *Phys. Rev. Lett.* **92** 016101

[38] Wahlström E, Ekvall I, Olin H and Walldén L 1998 Long-range interaction between adatoms at the Cu(1 1 1) surface imaged by scanning tunneling microscopy *Appl. Phys.* A **66** S1107–10

[39] Hyldgaard P and Persson M 2000 Long-range adsorbate-adsorbate interactions mediated by a surface-state band *J. Phys.: Condens. Matter* **12** L13–9

[40] Negulyaev N N, Stepanyuk V S, Niebergall L, Hergert W, Fangohr H and Bruno P 2006 Self-organization of Ce adatoms on Ag(1 1 1): a kinetic Monte Carlo study *Phys. Rev.* B **74** 035421

[41] Negulyaev N N, Stepanyuk V S, Hergert W, Fangohr H and Bruno P 2006 Effect of long-range adsorbate interactions on the atomic self-assembly on metal surfaces *Surf. Sci.* **600** L58–61

[42] Stepanyuk V A, Niebergall L, Baranov A N, Hergert W and Bruno P 2006 Long-range electronic interactions between adatoms on transitionmetal surfaces *Comput. Mater. Sci.* **35** 272–4

[43] Nanayakkara S U, Sykes E C H, Fernández-Torres L C, Blake M M and Weiss P S 2007 Long-range electronic interations at a high temperature: bromine adatom islands on Cu(1 1 1) *Phys. Rev. Lett.* **98** 206108

[44] Kulawik M, Rust H-P, Heyde M, Nilius N, Mantooth B A, Weiss P S and Freund H-J 2005 Interaction of CO molecules with surface state electrons on Ag(1 1 1) *Surf. Sci.* **590** L253–8

[45] Sykes E CH, Han P and Weiss P S 2003 Molecule/metal surface interactions evidenced quantum mechanically via tip-induced CS_2 interaction with Friedel oscillations on Au{1 1 1} *J. Phys. Chem.* B **107** 5016–21

[46] Wang Y, Ge X, Manzano C, Kröger J, Berndt R, Hofer W A, Tang H and Cerda J 2009 Supramolecular patterns controlled by electron interference and direct intermolecular interactions *J. Am. Chem. Soc.* **131** 10400–2

[47] Yokoyama T, Takahashi T and Shinozaki K 2007 Quantitative analysis of long-range interactions between adsorbed dipolar molecules on Cu(1 1 1) *Phys. Rev. Lett.* **98** 206102

[48] Crommie M F, Lutz C P and Eigler D M 1993 Confinement of electrons to quantum corrals on a metal surface *Science* **262** 218–20

[49] Crommie M F, Lutz C P, Eigler D M and Heller E J 1995 Quantum corrals *Physica* D **83** 98–108

[50] Kliewer J, Berndt R and Crampin S 2001 Scanning tunneling spectroscopy of electron resonators *New J. Phys.* **3** 22

[51] Manoharan H C, Lutz C P and Eigler D M 2000 Quantum mirages formed by coherent projection of electronic structure *Nature* **403** 512–5

[52] Crampin S, Jensen H, Kröger J, Limot L and Berndt R 2005 Resonator design for use in scanning tunneling spectroscopy studies of surface electron lifetimes *Phys. Rev.* B **72** 035443

[53] Kliewer J, Berndt R and Crampin S 2000 Controlled modification of individual adsorbate electronic structure *Phys. Rev. Lett.* **85** 4936–9

[54] Stepanyuk V S, Niebergall L, Hergert W and Bruno P 2005 *Ab initio* study of mirages and magnetic interactions in quantum corrals *Phys. Rev. Lett.* **94** 187201

[55] Stepanyuk V S, Negulyaev N N, Niebergall L and Bruno P 2007 Effect of quantum confinement of surface electrons on adatom-adatom interactions *New J. Phys.* **9** 388

[56] Negulyaev N N, Stepanyuk V S, Niebergall L, Bruno P, Herget W, Repp J, Rieder K-H and Meyer G 2008 Direct evidence for the effect of quantum confinement of surface-state electrons on atomic diffusion *Phys. Rev. Lett.* **101** 226601

[57] Nilius N, Wallis T M and Ho W 2002 Development of 1D band structure in artificial gold chains *Science* **297** 1853–6

[58] Wallis T M, Nilius N and Ho W 2002 Electronic density oscillations in gold atomic chains assembled atom by atom *Phys. Rev. Lett.* **89** 236802

[59] Nilius N, Wallis T M and Ho W 2004 Building alloys from single atoms: Au-Pd chains on NiAl(1 1 0) *J. Phys. Chem.* B **108** 14616–9

[60] Chen C, Bobisch C A and Ho W 2009 Visualization of Fermi's golden rule through imaging of light emission from atomic silver chains *Science* **325** 981–5

[61] Niebergall L, Rodary G, Ding H F, Sander D, Stepanyuk V S, Bruno P and Kirschner J 2006 Electron confinement in hexagonal vacancy islands: theory and experiment *Phys Rev.* B **74** 195436

[62] Kröger J, Limot L, Jesen H, Berndt R, Crampin S and Pehlke E 2005 Surface state electron dynamics of clean and adsorbate-covered metal surfaces studied with the scanning tunneling microscope *Prog. Surf. Sci.* **80** 26–48

[63] Li J, Schneider W-D, Crampin S and Berndt R 1999 Tunnelling Spectroscopy of surface state scattering and confinement *Surf. Sci.* **422** 95–106

[64] Seufert K, Auwärter W, Garcia de Abajo F J, Ecija D, Vijayaraghavan S, Joshi S and Barth J V 2013 Controlled interaction of surface quantum-well electronic states *Nano Lett.* **13** 6130

[65] Pennec Y, Auwärter W, Schiffrin A, Weber-Bargioni A, Riemann A and Barth J V 2007 Supramolecular gratings for tuneable confinement of electrons on metal surfaces *Nat. Nanotechnol* **2** 99–103

[66] Schiffrin A, Reichert J, Auwärter W, Jahnz G, Pennec Y, Weber-Bargioni A, Stepanyuk V S, Niebergall L, Bruno P and Barth J V 2008 Self-aligning atomic strings in surface-supported biomolecular gratings *Phys. Rev.* B **78** 035424

[67] Whitesides G M, Mathias J P and Seto C T 1991 Molecular self-assembly and nanochemistry: a chemical strategy for the synthesis of nanostructures *Science* **254** 1312–9

[68] Barth J V, Weckesser J, Cai C, Günter P, Bürgi L, Jeandupeux O and Kern K 2000 Building supramolecular nanostructures at surfaces by hydrogen bonding *Angew. Chem. Int. Ed.* **39** 1230–4

[69] Theobald J A, Oxtoby N S, Phillips M A, Champness N R and Beton P H 2003 Controlling molecular deposition and layer structure with supramolecular surface assemblies *Nature* **424** 1029–31

[70] Otero R, Schöck M, Molina L M, Lægsgaard E, Stensgaard I, Hammer B and Besenbacher F 2005 Guanine quartet networks stabilized by cooperative hydrogen bonds *Angew. Chem. Int. Ed.* **44** 2270–5

[71] Llanes-Pallas A, Matena M, Jung T, Prato M, Stöhr M and Bonifazi D 2008 Trimodular engineering of linear supramolecular miniatures on Ag(1 1 1) surfaces controlled by complementary triple hydrogen bonds *Angew. Chem. Int. Ed.* **47** 7726–30

[72] Yokoyama T, Yokoyama S, Kamikado T, Pkuno Y and Mashiko S 2001 Selective assembly on a surface of supramolecular aggregates with controlled size and shape *Nature* **413** 619–21

[73] Wintjes N, Hornung J, Lobo-Checa J, Voigt T, Samuely T, Thilgen C, Stöhr M, Diederich F and Jung T A 2008 Supramolecular synthons on surfaces: controlling dimensionality and periodicity of tetraarylporphyrin assemblies by the interplay of cyano and alkoxy substituents *Chem. Eur. J.* **14** 5794–802

[74] Stöhr M, Boz S, Schär M, Nguyen M-T, Pignedoli C A, Passerone D, Schweizer W B, Thilgen C, Jung T A and Diederich F 2011 Self-assembly and 2D spontaneous resolution of cyano-functionalized [7]helicenes on Cu(1 1 1) *Angew. Chem. Int. Ed.* **50** 9982–6

[75] Lin N, Dmitriev A, Weckesser J, Barth J V and Kern K 2002 Real-time single-molecule imaging of the formation and dynamics of coordination compounds *Angew. Chem. Int. Ed.* **41** 4779–83

[76] Barth J V 2009 Fresh perspectives for surface coordination chemistry *Surf. Sci.* **603** 1533–42

[77] Kley C S, Čechal J, Kumagai T, Schramm F, Ruben M, Stepanow S and Kern K 2012 Highly adaptable 2D metal-organic coordination networks on metal surfaces *J. Am. Chem. Soc.* **134** 6072–5

[78] Beniwal S, Chen S, Kunkel D A, Hooper J, Simpson S, Zurek E, Zeng X C and Enders A 2014 Kagome-like lattice of π–π stacked 3-hydroxyphenalenone on Cu(1 1 1) *Chem. Commun.* **50** 8659–62

[79] Fendt L-A, Stöhr M, Wintjes N, Enache M, Jung T A and Diederich F 2009 Modification of supramolecular binding motifs induced by substrate registry: formation of self-assembled macrocycles and chain-like patterns *Chem. Eur. J.* **15** 11139–50

[80] Heim D, Seufert K, Auwärter W, Aurisicchio C, Fabbro C, Bonifazi D and Barth J V 2010 Surface-assisted assembly of discrete porphyrin-based cyclic supramolecules *Nano Lett.* **10** 122–8

[81] Heim D, Écija D, Seufert K, Auwärter W, Aurisicchio C, Fabbro C, Bonifazi D and Barth J V 2010 Self-assembly of flexible 1D coordination polymers on metal surfaces *J. Am. Chem. Soc.* **132** 6783–90

[82] Koepf M, Chérioux F, Wytko J A and Weiss J 2012 1D and 3D surface-assisted self-organization *Coord. Chem. Rev.* **256** 2872–92

[83] Liang H, He Y, Ye Y, Xu X, Cheng F, Sun W, Shao X, Wang Y, Li J and Wu K 2009 2D molecular porous networks constructed by surface assembling *Coord. Chem. Rev.* **253** 2959–79

[84] Matena M *et al* 2010 Aggregation and contingent metal/surface reactivity of 1,3,8,10-Tetraazaperopyrene (TAPP) on Cu(1 1 1) *Chem. Eur. J.* **16** 2079–91

[85] Bonifazi D, Mohani S and Llanes-Pallas A 2009 Supramolecular chemistry at interfaces: molecular recognition on nanopatterned porous surfaces *Chem. Eur. J.* **15** 7004–25

[86] Li M, Zeng Q D and Wang C 2011 Self-assembled supramolecular networks at interfaces: molecular immobilization and recognition using nanoporous templates *Sci. China Phys. Mech. Astron.* **54** 1739–48

[87] Zhang X, Zeng Q and Wang C 2013 Molecular templates and nano-reactors: 2D hydrogen bonded supramolecular networks on solid/liquid interfaces *RSC Adv.* **3** 11351–66

[88] Perdigão L M A, Perkins E W, Ma J, Staniec P A, Rogers B L, Champness N R and Beton P H 2006 Bimolecular networks and supramolecular traps on Au(1 1 1) *J. Phys. Chem.* B **110** 12539–42

[89] Karmel H J, Chien T Y, Demers-Carpentier V, Garramone J J and Hersam M C 2014 Self-assembled 2D heteromolecular nanoporous molecular arrays on epitaxial graphene *J. Phys. Chem. Lett.* **5** 270–4

[90] Korolkov V V, Svatek S A, Allen S, Roberts C J, Tendler S J B, Taniguchi T, Watanabe K, Champness N R and Beton P H 2014 Bimolecular porous supramolecular networks deposited from solution on layered materials: graphite, boron nitride and molybdenum disulphide *Chem. Commun.* **50** 8882–5

[91] Lackinger M and Heckl W M 2009 Carboxylic acids: versatile building blocks and mediators for 2D supramolecular self-assembly *Langmuir* **25** 11307–21

[92] Ye Y, Sun W, Wang Y, Shao X, Xu X, Cheng F, Li J and Wu K 2011 A unified model: self-assembly of trimesic acid on gold *J. Phys. Chem.* C **111** 10138–41

[93] Iancu V, Braun K-F, Schouteden K and Van Haesendonck C 2013 Probing the electronic properties of trimesic acid nanoporous networks on Au(1 1 1) *Langmuir* **29** 11593–9

[94] Elemans J A A W, Lei S and De Feyter S 2009 Molecular supramolecular networks on surfaces from 2D crystal engineering to reactivity *Angew. Chem. Int. Ed.* **48** 7298–332

[95] Schlickum U *et al* 2007 Metal-organic honeycomb nanomeshes with tunable cavity size *Nano Lett.* **7** 3813–7

[96] Studener F, Müller K, Marets N, Bulach V, Hosseini M W and Stöhr M 2015 From hydrogen bonding to metal coordination and back: porphyrin-based networks on Ag(1 1 1) *J. Chem. Phys.* **142** 101926

[97] Dmitriev A, Spillmann H, Lin N, Barth J V and Kern K 2003 Modular Assembly of 2D metal-organic coordination networks at a metal surface *Angew. Chem. Int. Ed.* **42** 2670–3

[98] Stepanow S, Lingenfelder M, Dmitriev A, Spillmann H, Delvigne E, Lin N, Deng X, Cai C, Barth J V and Kern K 2004 Steering molecular organization and host-guest interactions using 2D nanoporous coordination systems *Nat. Mater.* **3** 229–33

[99] Stepanow S, Lin N, Payer D, Schlickum U, Klappenberger F, Zoppellaro G, Ruben M, Brune H, Barth J V and Kern K 2007 Surface-assisted assembly of 2D metal-organic networks that exhibit unusual threefold coordination symmetry *Angew. Chem. Int. Ed.* **46** 710–3

[100] Tait S L, Langner A, Lin N, Chandrasekar R, Fuhr O and Ruben M 2008 Assembling isostructural metal-organic coordination architectures on Cu (1 0 0), Ag (1 0 0) and Ag (1 1 1) substrates *ChemPhysChem* **9** 2495–9

[101] Abdurakhmanova N, Tseng T-C, Langner A, Kley C S, Sessi V, Stepanow S, and Kern K 2013 Superexchange-mediated ferromagnetic coupling in 2D Ni-TCNQ networks on metal surfaces *Phys. Rev. Lett.* **110** 027202

[102] Écija D *et al* 2013 Five-vertex Archimedean surface tessellation by lanthanide-directed molecular self-assembly *Proc. Natl Acad. Sci. USA* **110** 6678–81

[103] Walch H, Dienstmaier J, Eder G, Gutzler R, Schlögl S, Sirtl T, Das K, Schmittel M and Lackinger M 2011 Extended 2D metal-organic frameworks based on thiolate-copper coordination bonds *J. Am. Chem. Soc.* **133** 7909–15

[104] Faraggi M N, Jiang N, Gonzalez-Lakunza N, Langner A, Stepanow S, Kern K, and Arnau A 2012 Bonding and charge transfer in metal-organic coordination networks on Au(1 1 1) with strong acceptor molecules *J. Phys. Chem.* C **116** 24558–65

[105] Gottardi S, Müller K, Moreno-López J C, Yildirim H, Meinhardt U, Kivala M, Kara A and Stöhr M 2014 Cyano-functionalized triarylamines on Au(1 1 1): Competing intermolecular versus molecule/substrate interactions *Adv. Mater. Interfaces* **1** 1300025

[106] Pham T A, Song F, Alberti M N, Nguyen M-T, Trapp N, Thilgen C, Diederich F and Stöhr M 2015 Heat-induced formation of 1D coordination polymers on Au(1 1 1): an STM study *Chem. Commun.* **51** 14473

[107] Lingenfelder M A, Spillmann H, Dmitriev A, Stepanow S, Lin N, Barth J V and Kern K 2004 Towards surface-supported supramolecular architectures: Tailored coordination assembly of 1,4-benzenedicarboxylate and Fe on Cu(1 0 0) *Chem. Eur.* J **10** 1913–9

[108] Heller E J, Crommie M F, Lutz C P and Eigler D 1994 Scattering and absorption of surface electron waves in quantum corrals *Nature* **369** 464

[109] Heller E J, Crommie M F, Lutz C P and Eigler D 1995 Quantum corrals *Physica* D **83** 98–108

[110] Fiete G A and Heller E J 2003 Colloquium: theory of quantum corrals and quantum mirages *Rev. Mod. Phys.* **75** 933

[111] Crampin S and Bryant O R 1996 Fully 3D scattering calculations of standing electron waves in quantum nanostructures: the importance of quasiparticle interactions *Phys. Rev.* B **54** R17367

[112] Kepcija N, Huang T-J, Klappenberger F and Barth J V 2015 Quantum confinement in self-assembled 2D nanoporous honeycomb networks at close-packed metal surfaces *J. Chem. Phys.* **142** 101931

[113] Myroshnychenko V, Carbo-Argibay E, Pastoriza-Santos I, Perez-Juste J, Liz-Marzan L M and Garcia de Abajo F J 2008 Modeling the optical response of highly faceted metal nanoparticles with a fully 3D boundary element method *Adv. Mater.* **20** 4288

[114] Lobo-Checa J, Matena M, Müller K, Dil J H, Meier F, Gade L H, Jung T A and Stöhr M 2009 Band formation from coupled quantum dots formed by a nanoporous network on a copper surface *Science* **325** 300–3

[115] Matena M, Björk J, Wahl M, Lee T-L, Zegenhagen J, Gade L H, Jung T A, Persson M and Stöhr M 2014 On-surface synthesis of a 2D porous coordination network: unraveling adsorbate interactions *Phys. Rev.* B **90** 125408

[116] Stöhr M, Wahl M, Galka C H, Riehm T, Jung T A and Gade L H 2005 Controlling molecular assembly in two dimensions: the concentration dependence of thermally induced 2D aggregation of molecules on a metal surface *Angew. Chem. Int. Ed.* **44** 7394–8

[117] Roushan P, Seo J, Parker C, Hor Y S, Hsieh D, Qian D, Richardella A, Hasan M Z, Cava R J and Yazdani A 2009 Topological surface states protected from backscattering by chiral spin texture *Nature* **460** 1106–10

[118] Cottin M C, Bobisch C A, Schaffert J, Jnawali G, Bihlmayer G and Möller R 2013 Interplay between forward and backward scattering of spin-orbit split surface states of Bi(1 1 1) *Nano Lett.* **13** 2717–22

[119] Klappenberger F, Kühne D, Krenner W, Silanes I, Arnau A, García de Abajo F J, Klyatskatya S, Ruben M and Barth J V 2009 Dichotomous array of chiral quantum corrals by a self-assembled nanoporous Kagomé network *Nano Lett.* **9** 3509–14

[120] Klappenberger F, Kühne D, Krenner W, Silanes I, Arnau A, García de Abajo F J, Klyatskatya S, Ruben M and Barth J V 2011 Tunable quantum dot arrays formed from self-assembled metal-organic networks *Phys. Rev. Lett.* **106** 026802

[121] Wang S, Wang W, Tan L Z, Li X G, Shi Z, Kuang G, Liu P N, Louie S G and Lin N 2013 Tuning 2D band structure of Cu(1 1 1) surface-sate electrons that interplay with artificial supramolecular architectures *Phys. Rev.* B **88** 245430

[122] Shchyrba A, Materns S C, Wäckerlin C, Matena M, Ivas T, Wadepohl H, Stöhr M, Jung T A and Gade L H 2014

Covalent assembly of a 2D molecular 'sponge' on a Cu(1 1 1) surface: confined electronic surface states in open and closed pores *Chem. Commun.* **50** 7628–31
[123] Lijnen E, Chibotaru L and Ceulemans A 2008 Radial rescaling approach for the eigenvalue problem of a particle in an arbitrarily shaped box *Phys. Rev.* E **77** 016702
[124] Pawin G, Wong K L, Kwon K-Y and Bartels L 2006 A homomolecular porous network at a Cu(1 1 1) surface *Science* **313** 961–2
[125] Wyrick J *et al* 2011 Do 2D 'nobel gas atoms' produce molecular honeycombs at a metal surface? *Nano Lett.* **11** 2944–8
[126] Cheng Z, Wyrick J, Luo M, Sun D, Kim D, Zhu Y, Lu W, Kim K, Einstein T L and Bartels L 2010 Adsorbates in a box: titration of substrate electronic states *Phys. Rev. Lett.* **105** 066104
[127] Pritchard J 1972 Chemisorption on copper *J. Vac. Sci. Technol.* **9** 895–900
[128] Raval R, Parker S F, Pemble M E, Hollins P, Pritchard J and Chester M A 1988 FT-RAIRS, EELS and LEED studies of the adsorption of carbon monoxide on Cu(1 1 1) *Surf. Sci.* **202** 353–77
[129] Wortmann B, van Voerden D, Graf P, Robles R, Abufager P, Lorente N, Bobisch C A and Möller R 2015 Reversible 2D phase transition driven by an electric field: visualization and control on the atomic scale *Nano Lett.* **16** 528–533
[130] Cheng Z, Luo M, Wyrick J, Sun D, Kim D, Zhu Y, Lu W, Kim K, Einstein T L and Bartels L 2010 Power of confinement: adsorbate dynamics on nanometer-scale exposed facets *Nano Lett.* **10** 3700–3
[131] Pivetta M, Pacchioni G E, Schlickum U, Barth J V and Brune H 2013 Formation of Fe cluster superlattice in a metal-organic quantum-box network *Phys. Rev. Lett.* **110** 08610
[132] Nowakowska S *et al* 2015 Interplay of weak interactions in the atom-by-atom condensation of xenon within quantum boxes *Nat. Commun.* **6** 6071